Transonic Flow Analysis using Vision based Model Order Reduction and Application to 3D Wing Shape Optimization

Donggeon Lee[1], Kwangshun Shim[1], Seongim Choi[2]

[1] Master's Program, Gwangju Institute of Science and Technology (GIST), Gwangju, 61005, Republic of Korea
[2] Associate Professor, Gwangju Institute of Science and Technology (GIST), Gwangju, 61005, Republic of Korea

Keywords: Condition U-Net, Residual block, Free-form deformation, shock optimization

Abstract.
In this study, shock optimization for the Onera M6 wing is conducted under flow conditions of Mach 0.83 and an angle of attack of 3.06 degrees. The computational fluid dynamics (CFD) open-source software Stanford University Unstructured (SU2) is used for the flow field analysis of the Onera M6 wing. To validate the CFD method, a comparison with experimental data is performed. The surrogate models used in the optimization process are Conditional U-Net with residual blocks and Deep Neural Network (DNN)**.** Each model is utilized for reconstructing the pressure coefficient (Cp) of the entire grid points and predicting aerodynamic coefficients. In the optimization process, aerodynamic coefficients are used as constraints, while the pressure coefficient is used as the objective function. For model training, the Free Form Deformation (FFD) method is applied to deform the initial wing shape, generating 836 training datasets**,** with 46 datasets used for testing**.** The Non-dominated Sorting Genetic Algorithm II (NSGA-II) algorithm is employed for optimization. As a result, the lambda shock, which occurs in the original shape, either disappears or shifts its position. However, a reduction in drag coefficient was not achieved.

1. Introduction

Changes in the airfoil or wing shape of an aircraft significantly influence its aerodynamics, determining key performance metrics such as range and fuel efficiency. Consequently, optimizing these shapes through high-accuracy aerodynamic analyses is essential. However, directly employing high-fidelity Computational Fluid Dynamics (CFD) methods in the optimization process is nearly impossible due to the immense computational time and memory requirements associated with conducting hundreds of thousands of CFD simulations. To overcome this limitation, surrogate models capable of replacing high-fidelity CFD during the optimization process are required, as well as reduced-order models (ROMs) that can efficiently calculate the entire flow field on a per-second basis. Convolutional Neural Networks (CNNs), inspired by the structure of the human visual system, are particularly effective at recognizing images and learning patterns. They are widely used in computer vision applications such as autonomous vehicles and facial recognition.

Prominent CNN-based models include ResNet, GoogleNet, and VGG, which were introduced through the ImageNet competition. ResNet employs residual blocks for residual learning, resolving issues like gradient vanishing or exploding. U-Net, first developed by Ronneberger et al. [1], has been applied to aerodynamic flow predictions, such as predicting three-dimensional flow fields [2] and compressible flow fields around supersonic airfoils [3]. In this study, the U-Net architecture is enhanced by incorporating residual blocks, utilizing it as a ROM during the optimization process. Additionally, DNN-based regression model is used to predict lift and drag coefficients based on design variables.

To generate various mesh for the surrogate model, the deformation module in SU2 was utilized. A direct search genetic algorithm without gradient sensitivities was used as the optimization algorithm. This approach is capable of handling multiple objectives and constraints, with the Non-dominated Sorting Genetic Algorithm II (NSGA-II) [4] employed for its simplicity. To achieve a shock-free Onera M6 Wing, the objective function is defined as the instantaneous rate of change of the Cp value in a selected wing section, while aerodynamic coefficients are used as constraints.

2. Method

2.1. Data Generation

The mesh used in the optimization process is shown in Figure 1. According to mesh convergence and CFD result with fine wake refinement mesh, under current flow condition, there was no significant wake formation. Therefore, wake refinement was set to 0.09mm. The mesh of wing surface consists of 59,928 cells, and the flow field does 3,454,027. The SU2 solver was employed to conducted Reynolds-Averaged Navier-Stokes (RANS) with SST(V2003m) turbulence model. And viscosity was modelled using the Sutherland law while conductivity was assumed to follow a constant Prandtl number.

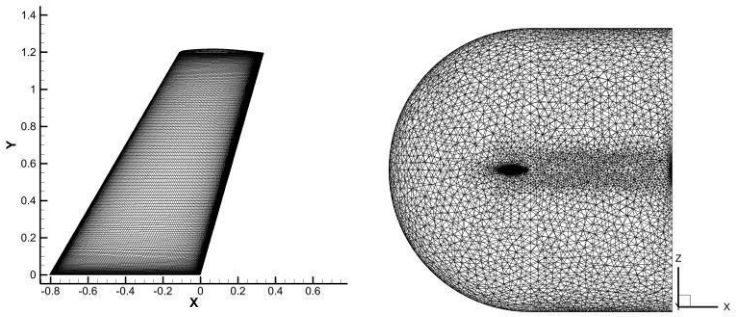

Figure 1. Computational domain of ONERA M6 wing

2.2. Shape Variation by Free Form Deformation

FFD is a parameterization technique first proposed by Sederberg and Parry in 1986 [5]. FFD essentially defines a lattice that encompasses the object and deforms the object by moving the control points of the lattice. In three-dimensional space, the lattice consists of $(l+1) \times (m+1) \times (n+1)$ control points. In this study, l, m, and n are set to 11, 7, and 1, respectively, resulting in 192 control points. FFD can be defined using Bezier or B-spline curves. The bezier curve was used to generate data for an aerodynamically continuous wing surface. To reduce design space, 30 control points (15 control points on the upper surface and 15 on the lower) were selected from 192 as shown in Figure 2. Each design variables was constrained to a maximum variation of ±0.25. Latin Hypercube Sampling algorithm was adopted to generate a dataset of 882 wing surface. The seed number was fixed at 1 for reproducibility. Figures 3 illustrates selected examples of FFD.

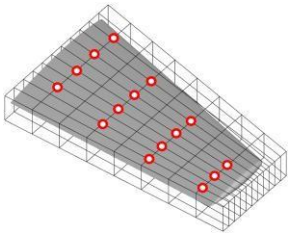

Figure 2. FFD block of wing (Red mark: active control points)

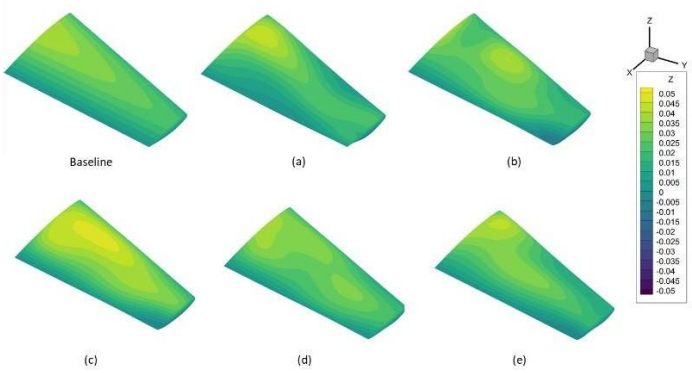

Figure 3. Selected examples of free form deformation

2.3. Surrogate Model

First included in ResNet in 2015, the residual block's purpose is to add the input before each layer is processed and, at the conclusion of the computation, to the output. A residual block is a part that learns the residual, or difference, between the input and output of a neural network. By lowering the quantity of data that each layer must learn, residual learning successfully resolves problems like gradient disappearing or exploding that may arise as network depth grows.

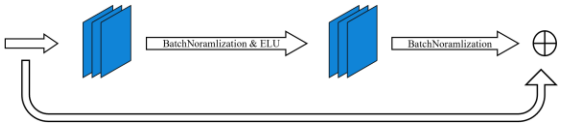

Figure 4. Operation of residual block

The structure of Conditional U-Net with residual block, which adds conditions to the U-Net architec ture, is as shown in Figure 5. In the encoder, the input consists of x, y, and z coordinate values, while t he condition takes the design variables of the FFD that are related to the input x, y, and z. The model p redicts the pressure coefficient at each grid point based on both the input and the condition.

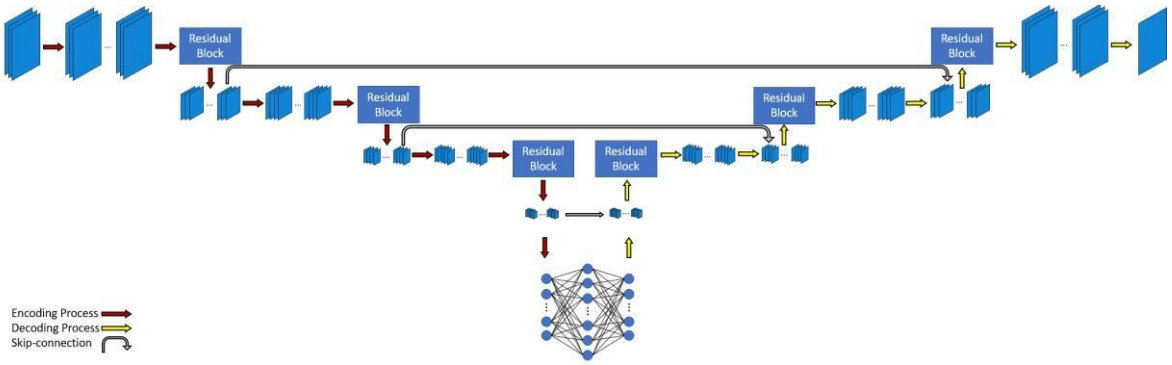

Figure 5. Structure of Conditional U-Net with residual block

The structure of the DNN used for aerodynamic coefficient prediction is shown in Figure 6. The network takes 30 design variable values as input and passes them through dense layers with 64, 128, 64, and 32 nodes, respectively. Finally, it predicts two output values: the drag coefficient and the lift coefficient. The activation function used in the hidden layers is the Exponential Linear Unit (ELU).

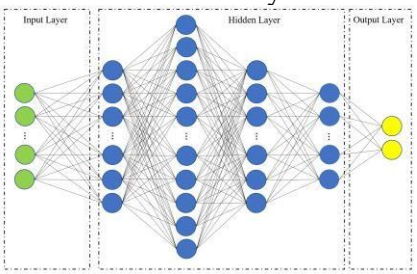

Figure 6. Structure of DNN

3. Validation of CFD Solution

The CFD results for the ONERA M6 wing reveal the presence of two shocks, one near the leading edge and another at the mid-chord, as illustrated in Figure 7. To validate the numerical simulation, the pressure coefficient (C_p) distributions extracted from the CFD analysis are compared against experimental data provided by Schmitt & Charpin [6] at sections y/b=0.2, 0.8, and 0.99(b= 1196.3mm; full span). As shown in Figure 8, the numerical results agree with the experimental measurements, demonstrating the accuracy of the computational approach.

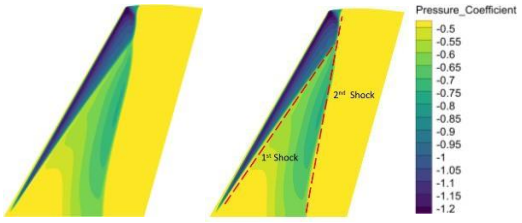

Figure 7. CFD result of ONERA M6

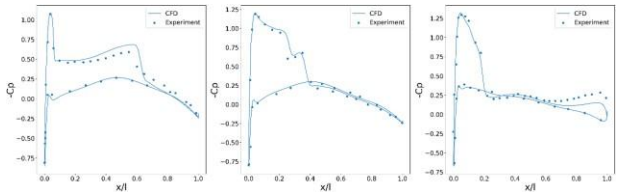

Figure 8. Cp plot of Wing Section (from left side to right, y/b= 0.2, 0.8, 0.99)

Figure 9 presents the results of the CFD solution and the predicted flow field from the model. As shown in the absolute error plot, the error magnitude increases in the regions where the lambda shock occurs. The increase in error near the lambda shock region is due to the heightened nonlinearity of the data.

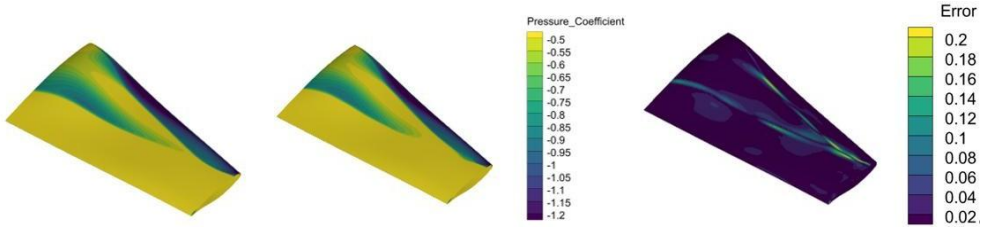

(a) (b) (c)

Figure 9. Full order model CFD (a), Prediction (b), Absolute error (c)

4. Optimization Process

The optimization process is illustrated in Figure 10. The initial design variable is processed through SU2's deformation module, where it is transformed into x, y, and z coordinates. These coordinates are then fed into a U-Net with residual blocks to reconstruct the flow field. DNN takes the design variable values as input to predict the aerodynamic coefficients. The objective function is set as the squared sum of the instantaneous pressure coefficient variations over a specific wing section. The constraints are based on the lift and drag coefficients. As a result of the optimization process, the optimized design variable values are obtained. Through post-processing, these values are converted into x, y, and z coordinates, and the solution is evaluated to determine the presence of shocks and the aerodynamic coefficients.

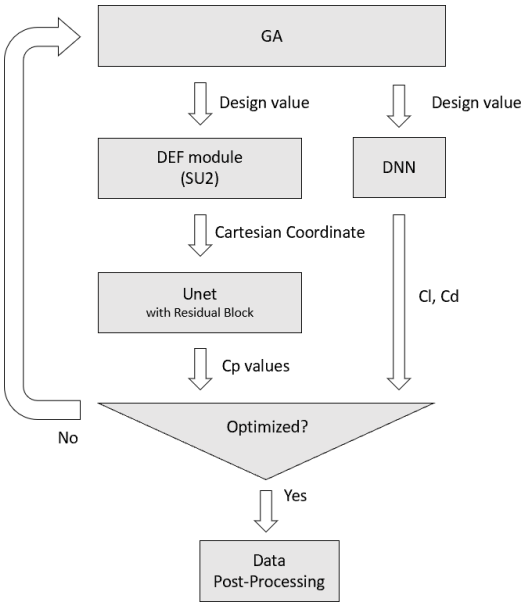

Figure 10. Schematic diagram of optimization process

5. Results

(a) (b) (c)

Figure 11. Optimal Solutions; (a) similar (b) bottom (c) dual

The optimization results are presented in Figure 11. As shown in Figure 11 (a), the optimized shape closely resembles the baseline configuration. However, in some cases, such as (b), the shock-induced flow separation region shifts closer to the wing root. (c) demonstrates a reduction in the area of the first shock, but this comes at the cost of an intensified second shock. In all cases, the lift coefficient remained at 0.27, satisfying the initial constraint; however, no reduction in the drag coefficient was achieved.

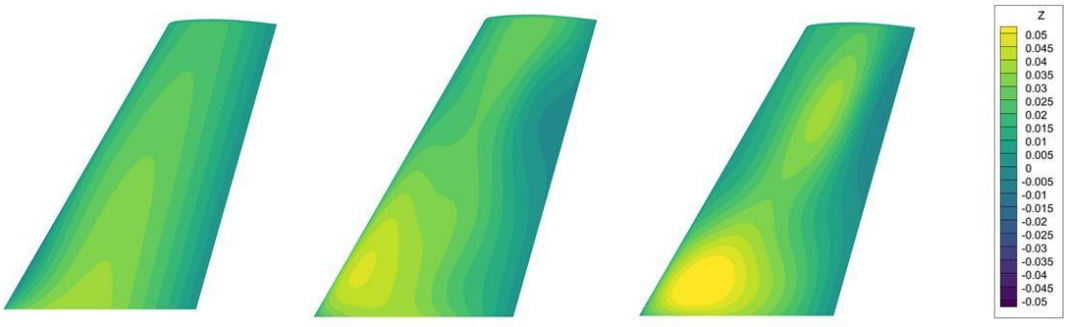

(a) (b) (c)

Figure 12. Geometry of optimal solutions; (a) similar (b) bottom (c) dual

The optimization results indicate that the shock position was modified by introducing localized bumps in certain regions, as shown in Figure 12. The shock primarily formed in areas where the flow accelerated along the bump, and it was observed that larger bumps resulted in stronger shock intensity. In Figure 12(a), the optimized shape closely resembles the baseline configuration, with only minor modifications near the root region. In contrast, (b) features a more pronounced bump near the root, which effectively shifts the shock-induced flow separation point closer to the root. In (c), an additional bump appears near the tip, leading to the formation of two distinct shock waves along the span.

6. Conclusion

The lack of drag reduction in the optimization results can be attributed to several potential factors. First, the dataset of 882 samples may be insufficient to fully represent the variations in the 30-dimensional control space. As a result, even if the NSGA-II successfully identified the optimal design within the surrogate model, the surrogate model itself may not have accurately predicted the true aerodynamic performance. Second, there are inherent limitations in the objective function. The current optimization process is based on variations in the pressure coefficient at only three cross-sections. However, further discussion is needed to determine whether these specific sections are truly representative of the entire wing's aerodynamic characteristics. Third, in the current Free-Form Deformation (FFD) framework, both the upper and lower surfaces of the wing are subject to deformation. However, the optimization results suggest that maintaining the lower surface unchanged yields superior aerodynamic performance. The inclusion of lower surface modifications in the optimization process may have led to suboptimal results, potentially degrading overall aerodynamic efficiency.

Future studies should incorporate the following improvements. First, control points should be assigned only to the upper surface of the wing, while deformation of the lower surface should be restricted. This approach will reduce the design space, allowing the surrogate model to function more effectively. Additionally, the objective function will be refined by conducting a parametric study to identify and select the most critical cross-section locations for optimization.

7. Acknowledgments

This work was supported by the Technology Innovation Program (or Industrial Strategic Technology Development Program) – Development high-accuracy prediction method of phase change, BOR, and pressure change in the cargo hold of LNG/LH2 ships in consideration of the operating environment, 20026368, funded by the Ministry of Trade, Industry & Energy (MOTIE, Korea).

8. References

[1] Ronneberger, O., Fischer, P. and Becker, A., "U-Net: Convolutional networks for biomedical image segmentation," Medical Image Compution and Computer-Assisted Intervention, November 2015, p.234-241.

[2] Zhu, J., Wang, S., Wei, N. and Xu, Q.Z., "A three-dimensional flow field reconstruction method of wing based on SE-3DUnet," 35th Chinese Control and Decision Conference, 2023, p.923-928.

[3] Zhu, Z., Zhao, G. and Zhao, Q., March 2024, Physics of Fluids, "Fast and high-precision compressible flowfield inference method of transonic airfoils based on attention UNet," Vol.36, p.1-24.

[4] Deb, K., Pratap, A., Agarwal, S., & Meyarivan, T. A. M. T. (2002). A fast and elitist multiobjective genetic algorithm: NSGA-II. IEEE transactions on evolutionary computation, 6(2), 182-197. doi: 10.1109/4235.996017

[5] T. W. Sederberg and S. R. Parry, "Free-form deformation of solid geometric models," *Proceedings of the 13th Annual Conference on Computer Graphics and Interactive Techniques*, Dallas, TX, USA, 18–22 August 1986, pp. 151–160.

[6] V. Schmitt, F. Charpin, *Pressure Distributions on the ONERA-M6-Wing at Transonic Mach Numbers*, Experimental Data Base for Computer Program Assessment, Report of the Fluid Dynamics Panel Working Group 04, AGARD AR 138, May 1979.